DSC-Vol. 59

MICRO-ELECTRO-MECHANICAL SYSTEMS (MEMS)

MICROSCALE THERMAL PHENOMENA IN ELECTRONIC SYSTEMS

C. T. Avedisian, Y. Bayazitoglu, K. Cole, K. Goodson, G. Kowalski, and A. Majumdar

APPLICATIONS OF MICROFABRICATION TO FLUID MECHANICS

K. Breuer, P. Bandyopadhyay and M. Gad-el-Hak

MECHANICS IN MICRO-ELECTRO-MECHANICAL SYSTEMS (MEMS)

G. C. Johnson and P. A. Krulevitch

MICROMECHANICAL SYSTEMS

C.-J. Kim, J. Jara-Almonte, A. P. Pisano, A. P. Lee, and T. Hirano

1996 ASME INTERNATIONAL MECHANICAL ENGINEERING CONGRESS AND EXPOSITION

DSC-Vol. 59, Microelectromechanical Systems (MEMS)
ASME 1996

AN APPROACH TO MACROMODELING OF MEMS FOR NONLINEAR DYNAMIC SIMULATION

G. K. Ananthasuresh, Raj K. Gupta, and Stephen D. Senturia

Microsystems Technology Laboratories
Massachusetts Institute of Technology
Cambridge, MA 02139

ABSTRACT

The method of linear normal mode summation is utilized here to construct reduced order macromodels to perform the nonlinear dynamic analysis of microelectromechanical devices and systems (MEMS). The validity of the approach is illustrated with the example of a doubly clamped beam under electrostatic actuation. Using the reduced order macromodel, it is possible to observe nonlinear effects such as the frequency shift due to a DC bias voltage, and the amplitude-dependence of resonance frequency. The undamped *dynamic pull-in voltage* is found to be about 9% less than the quasi-static pull-in voltage. The dynamic simulation results of the macromodel are compared with those of the complete model, and it is noted here that linear normal modes provide an adequate basis to carry out the dynamic analysis with enormous computational advantage while not losing accuracy. The simulation results are also validated with the experimentally measured data for the dynamic and static pull-in voltages, and the time to pull in at voltages beyond the pull-in voltage.

INTRODUCTION

With the increased development of and usage of microsystems that operate in the dynamic regime (e.g., micro opto-mechanical devices (Apte et al., 1994), and accelerometers (Spangler and Kemp, 1995)), there is a perceivable need for efficient algorithms and software tools to simulate the dynamics of MEMS devices. For example, electrostatically actuated MEMS devices exhibit nonlinear dynamic behavior as the electrostatic force couples nonlinearly with the elastomechanical behavior. There are also other nonlinear coupling effects such as the fluid damping and fluid back-pressure. Furthermore, the devices can also exhibit geometric nonlinearity associated with large deformations. The accurate simulation of the complete system requires an enormous amount of computation as is evident from the previously reported studies on the dynamic simulation of specific devices (Ulrich et al., 1995). Shi et al. (1996) used the modified Newmark method and a hybrid BEM/FEM approach to perform the dynamic simulation of electromechanical microtweezers. Tilmans (1993) obtained approximate analytical expression for DC bias dependent resonance frequency of electromechanical structures using Rayleigh's Quotient and assumed mode shapes. The focus of this paper is an exploration of a method for decreasing the computation without compromising on the accuracy.

The meshed models used in the quasi-static simulation of electrostatically actuated MEMS devices usually require a large number of nodes to give sufficiently accurate results. Simulation of the dynamic behavior using the same models would imply solving a large number of nonlinearly coupled, second order differential equations in addition to the repeated computations associated with the estimation of electrostatic and fluid forces. Using the *normal mode summation method* (Thomson, 1988), we present here an approach for the creation of reduced order *macromodels* (Senturia, 1995) for the dynamic analysis which results in enormous decrease in computation time (from several hours to a few minutes) without losing accuracy. We demonstrate the efficacy of the method by comparing the computation time and accuracy for the explicit computation of the complete model with those for the macromodel, using the simple example of a doubly clamped beam under electrostatic actuation. We also demonstrate the validity of the simulations by comparing them with the experimentally measured data for dynamic and static pull-in voltages, and the time to pull in at voltages beyond the pull-in voltage.

NORMAL MODE SUMMATION METHOD

In the normal mode summation method (Thomson, 1988), the deformed shape of the structure is expressed as a linear summation of the linear normal mode shapes. This results in the transformation from the nodal coordinates to the time-dependent coefficients of the mode shapes, called *modal coordinates*. It also eliminates the coupling in the inertia and stiffness terms. Under the reasonable assumption that higher modes have negligible effect on the system's response, a good reduced order macromodel can be constructed by using only the first few modes. Instead of the original system of N coupled equations (where N equals the total nodal degrees of freedom), we now solve P equations (where P equals the number of modes considered) and these equations are uncoupled in the inertia and stiffness terms. The number of modes considered determines both the accuracy and the computation time.

Description of the method

The normal mode method is applicable to both the 3-D finite element meshed models and lumped models where the mechanical structure is modeled appropriately using lumped masses and springs. In either case, the dynamic behavior of a system with N degrees of freedom is given by (neglecting damping):

$$[M]_{N\times N}\{\ddot{y}\}_{N\times 1} + [K]_{N\times N}\{y\}_{N\times 1} = \{f_e(y,t)\}_{N\times 1} \qquad (1)$$

where $[M]_{NxN}$ is the global inertia matrix, $[K]_{NxN}$ is the global stiffness matrix, $\{y\}_{Nx1}$ is the column vector of displacements, and $\{f_e(y,t)\}_{Nx1}$ is the nonlinear force, in this case, electrostatic force. The essence of normal mode summation method lies in transforming (1) to coordinates in modal space $\{q\}$, from the coordinates in the $\{y\}$ space using the following transformation:

$$\{y\}_{Nx1} = [S]_{NxN} \{q\}_{Nx1} \quad (2)$$

or equivalently,

$$\{y\}_{Nx1} = q_1 \{s_1\}_{Nx1} + q_2 \{s_2\}_{Nx1} + ... + q_N \{s_N\}_{Nx1} \quad (2a)$$

where [S] is an NxN matrix whose columns are the mode shape vectors, s_i (i = 1..N) of the system. After the above transformation and pre-multiplication of (1) by $[S]^T$, it results in a system of equations that is completely uncoupled on the left hand side.

$$[M_G]_{NxN} \{\ddot{q}\}_{Nx1} + [K_G]_{NxN} \{q\}_{Nx1} = [S]^T_{NxN} \{f_e(q,t)\}_{Nx1} \quad (3)$$

where $[M_G]_{NxN}$ and $[K_G]_{NxN}$ are diagonal matrices. Under the reasonable assumption that higher modes have negligible effect on the system, a truncated expansion of (2a) can be used to reduce the order of the system as shown below.

$$\{y\}_{Nx1} = q_1 \{s_1\}_{Nx1} + q_2 \{s_2\}_{Nx1} + ... + q_P \{s_P\}_{Nx1} \quad (4)$$

$$[M_G]_{PxP} \{\ddot{q}\}_{Px1} + [K_G]_{PxP} \{q\}_{Px1} = [S]^T_{PxN} \{f_e(q,t)\}_{Nx1} \quad (5)$$

The method derives its strength from the fact that a value of P that is much less than N is adequate in most cases. The value of P needs to be just as large as the number of dominant normal modes in the dynamic response of the system. The smaller the value of P, the better is the computational advantage. The "macromodel" of the system is now comprised of P modal coordinates $\{q\}$ and their associated generalized inertia and stiffness values.

VALIDITY OF THE APPROACH

For a reasonable value of P, Equation (5) is perfectly valid for linear systems, but its applicability to nonlinear systems is not readily apparent because of the nonlinear coupling terms on the right hand side of (5) and the geometric nonlinearity associated with large deformations. In order to study the validity of this approach, a simple example is considered and is described below.

Figure 1 and Table 1 contain the features and the dimensions of the electrostatically actuated doubly clamped beam analyzed to illustrate the effectiveness of the method. The dynamic equation of the beam including Osterberg's fringing-field correction [9] is given by the following:

$$\rho \ddot{y} + EI\, y'''' = \{ w \varepsilon_0 V^2 / (2g)^2 \} * (1 + 0.65\, g/w) \quad (6)$$

where

ρ = mass density per unit length of the beam

y = displacement of the beam in the transverse direction;

y'''' denotes the fourth derivative with respect to x

$\ddot{y}$ denotes the second derivative with respect to time

x = position along the longitudinal direction of the beam

E = Young's modulus of the material

I = Moment of inertia = $(wt^3/12)$ for rectangular cross-section

w = width of the beam

t = thickness of the beam

ε_0 = permittivity of free space = 8.854×10^{-12} Farads/m

V = applied voltage

g = gap between the beam and the ground electrode = $(g_0 - y)$

Using the finite element formulation, the beam was modeled with beam elements (Przemienickie, 1968) and the electrostatic force was computed using the parallel-plate approximation with a fringing field correction. The resulting system of dynamical equations were modeled and integrated using the Runge-Kutta scheme in MATLAB (1993). For a large signal DC voltage (12 V) and a small signal AC voltage actuation (2 V at 111.4 KHz), Figures 2a and 2b compare the undamped displacement of the mid-point of the beam in the complete model $d_c(t)$, and that of a four-mode macromodel $d_m(t)$. The percent relative error, computed as $100*(d_c(t)-d_m(t)) / \max(d_c(t))$ and shown in Figure 2c, has an average value of 3.58E-2 with a standard deviation of 3.42E-2 over the entire time-interval. The huge improvement in computation time can be seen in Table 2 which shows the CPU time required for the complete model solution using 20 beam elements and 30 elements, and macromodel solutions using 4 and 8 modes for the same.

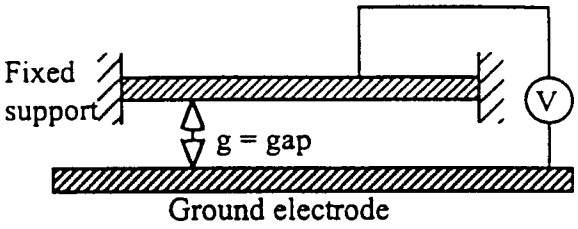

Figure 1 Doubly clamped beam under electrostatic actuation

Length = 80 um
Width = w = 10 um
Thickness = t = 0.5 um
Initial gap = g_0 = 0.7 um
Young's modulus = E = 169 GPa
Mass density = ρ = 2231 Kg/m^3

Table 1 Physical and material properties of the beam

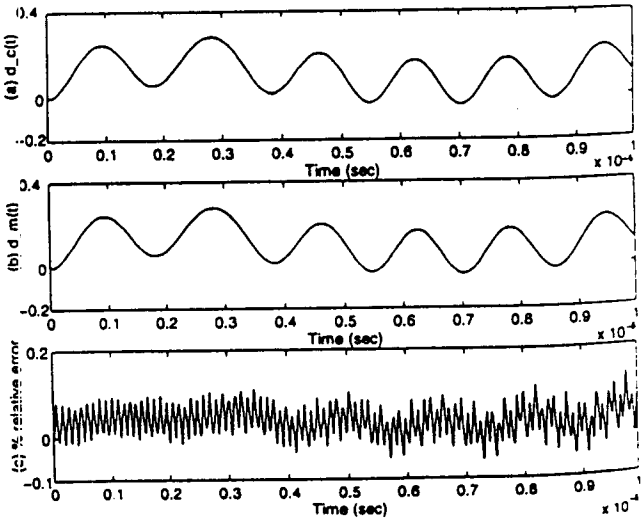

Figure 2 Displacement of the mid-point of the beam (in microns) (a) Complete model (b) 4-mode macromodel (c) % Relative error between the two models

To test sensitivity to higher order modes, electrodes were placed under only a few elements as shown in Figure 3, and the active electrodes were intermittently switched. Various patterns of actuation were simulated, and the same general agreement between the complete model and the macromodel was observed. For example, consider an actuation pattern in which the same combination of the DC and the AC voltage was applied, but only one electrode was activated at any given time. The active electrode was moved from left to right (Figure 3) after every 1 μsec. The simulation of the complete model took about 5 hours of CPU time to run for approximately 7.25 μsec of beam's dynamic response. The simulations that used 4-mode and 8-mode macromodels took less than 4 CPU minutes. The displacement of the mid point of the beam is shown in Figure 4a and 4b for the complete and 4-mode macromodel respectively. The percent relative error, as defined above and shown in Figure 4c, has a maximum value of 2% which is much higher than that of the previous case. This is due to the higher modes that were intentionally excited using the complex electrode and actuation pattern. Illustrated in Figures 5a and 5b are the time-dependent magnitudes of the modal coordinates corresponding to the first eight modes in the complete model simulation. It is apparent from the figure that more than four modes are required in this example. The responses due to the complete and 8-mode macromodels and the percent relative error between the two models are shown in Figures 6a, 6b and 6c respectively. The maximum error is now less than 0.25%.

Number of beam elements	Model	CPU time (seconds)
20	Complete model	12600
	4mode-macromodel	91
	8mode-macromodel	179
30	Complete model	43000
	4mode-macromodel	112
	8mode-macromodel	213

Table 2 Comparison of computation time for simulation

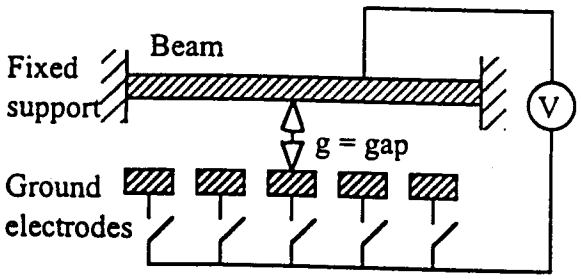

Figure 3 Beam with discrete electrodes to simulate complex actuation patterns and to excite higher modes

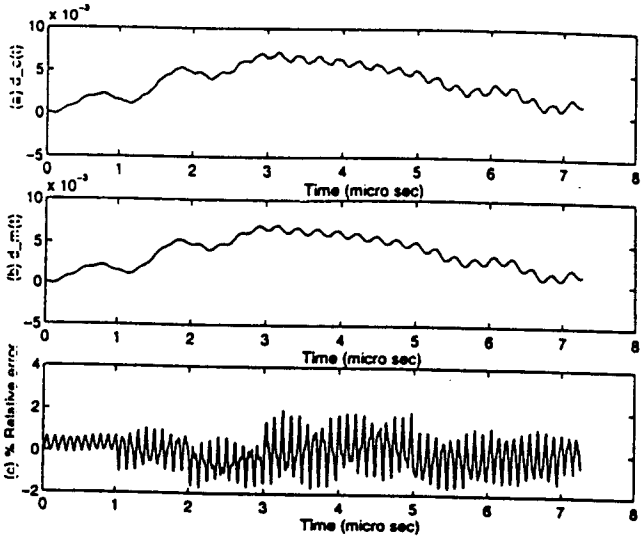

Figure 4 Displacement of the mid-point of the beam (in microns) (a) Complete model (b) 4-mode macromodel (c) % Relative error between the two models

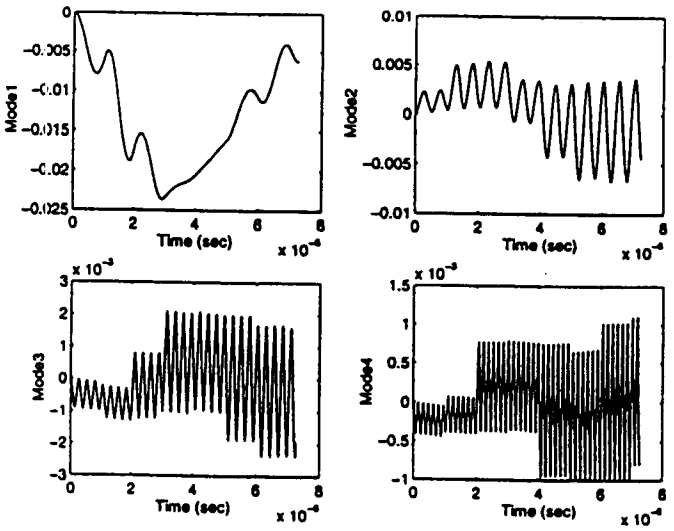

Figure 5a Time-variation of the modal coordinates in the simulation of the complete model

RESULTS AND DISCUSSION

For the beam example considered above, the electrostatic force acts like a nonlinear elastic foundation. Since the force acts in the direction of the motion, it indeed acts like a negative spring. The 'stiffness' of the 'foundation' is dependent not only on the deformation of the beam, but is also dependent on time as the voltage

is time-dependent. Many nonlinear effects can be observed in the dynamic response of the beam for different actuation voltages. Some of those effects are discussed in this section.

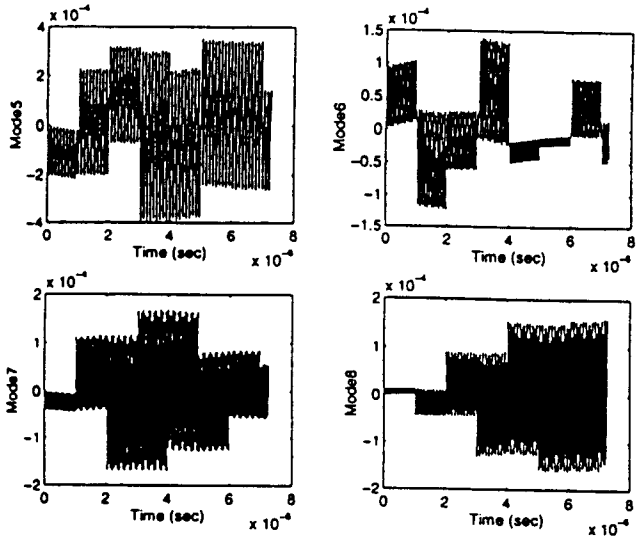

Figure 5b Time-variation of the modal coordinates in the simulation of the complete model (modes 5-8)

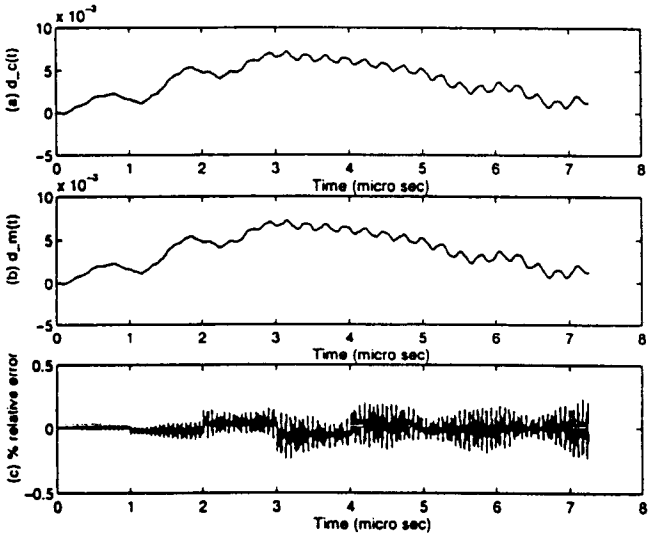

Figure 6 Displacement of the mid-point of the beam (in microns) (a) Complete model (b) 8-mode macromodel (c) % Relative error between the two models

Dynamic pull-in voltage

Electrostatically actuated structures reach an unstable point and pull-in onto the ground electrode when the DC bias voltage attains a value equal to the *pull-in voltage* of the structure. If the voltage is reduced after pull-in, the structure gets released at its *release voltage*. The pull-in and release voltages differ by some finite amount. Some MEMS devices use this phenomenon (e.g., diffraction-grating light valves (Apte et al., 1994)) to switch beam-structures between the two states. Accurate computation of the pull-in and release voltages is important in the design of such devices. This was done for the case of quasi-static application of the voltage using MIT's MEMCAD system (Gilbert et al., 1996). It was observed in the beam example considered here that the inertia of the beam influences the pull-in voltage. In order to study this effect, the DC bias voltage was applied as a ramp in a small interval until the required voltage is attained and then that value is maintained. The time for the ramp is varied and the limiting voltage is computed in each case. This limiting voltage is termed as the *dynamic pull-in voltage* here. The variation of the dynamic pull-in voltage with ramp-rate is shown in Figure 7. It can be seen that the beam has the lowest pull-in voltage of 13.7V when the DC voltage is applied with infinite ramp-rate, i.e., as a step. Using the pull-in formula reported in (Osterberg et al., 1994), the quasi-static pull-in voltage for this beam is computed as 15.17V which is shown as a black dot in the figure. Thus, there is a difference of about 9% in the quasi-static and the lowest undamped dynamic pull-in voltage.

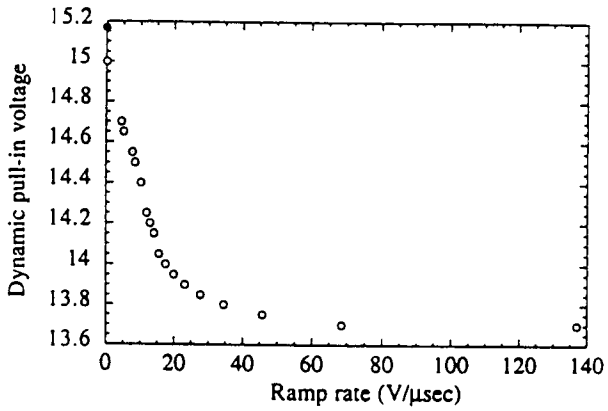

Figure 7 Dynamic pull-in voltage at different ramp rates

Comparison with experimental data. A noticeable difference between the quasi-static and dynamic pull-in voltages was experimentally observed by Gupta et al. (1996a). For a doubly clamped plolysilicon beam that was fabricated using MCNC's (1995) surface micromachining process, the quasi-static and dynamic voltages were measured to be 8.76V and 8.04V respectively. In this measurement the dynamic pull-in voltage is 8.2% less than the quasi-static pull-in voltage. A simulation performed using the macromodel indicated a difference of 7.8% between the quasi-static and dynamic pull-in voltages which are 7.26V and 6.69V respectively. The discrepancy between the experiment and the simulation is attributed to the change in geometry due to pre-buckled (i.e., below the buckling stress) deformation of the beam under the effect of compressive residual stress, and stress-stiffening

effect both of which were not taken into account in the simulation. Additional simulation results and the details of the construction of the macromodel for this beam are discussed in a later section. Although the damping effects might help decrease the difference in static and dynamic pull-in voltages, for accurate estimates it is still important to compute the pull-in and release voltages by accounting for inertia effects. The macromodels such as the one presented here offer a computationally efficient method to accomplish this.

Frequency-pulling effects due to DC bias

As noted above, the electrostatic force acts like a negative nonlinear spring. Consequently, the effective stiffness of the structure changes with deformation. This in turn causes the resonance frequency of the structure to shift. Since electrostatic force increases with increasing DC bias voltage, and thus increasing the deformation, the structure experiences spring-softening and the resonance frequency goes down as we increase the DC bias voltage. To determine the resonance frequency at a given DC bias voltage, the following simulation was performed. The simulation consisted of a step DC voltage with some artificially introduced damping for 10 μsec, and it was left undamped afterwards. The damping was introduced to force the beam to reach the steady-state deformation for the applied step DC voltage. As shown in Figure 8, after the beam reaches the steady-state, a small perturbation was given to the first mode of the beam and the simulation was continued by removing the damping. The frequency was measured from the resulting signal. By varying the DC voltage, several such simulations were carried out and the first resonance frequency was measured from the dynamic response of the beam. The plot of the first resonance frequency vs. DC bias voltage is shown in Figure 9. Starting with the original value of 700 KHz, the frequency tends to zero as the DC bias voltage approaches the pull-in voltage. Thus, the pronounced effect of the nonlinear 'electrostatic spring' effect is seen here.

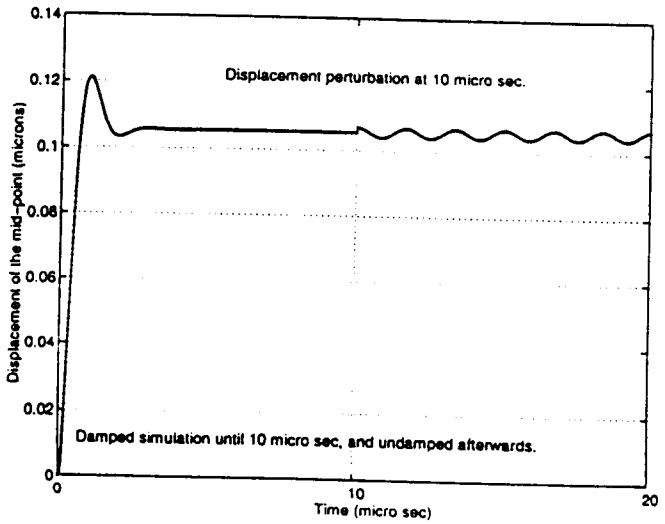

Figure 8 A simulation performed to determine the resonance frequency at 10 V DC bias

Amplitude-softening at a given DC bias

The downward shift in the resonance frequency occurs not only due to the DC bias voltage, but also due to the amplitude relative to the deformed state. This shift is significant when a small signal AC voltage is applied to the DC biased state and in controlling the beam around the DC operating point. It is possible to compute the amplitude dependence of the frequency for a given DC bias voltage by performing the simulation using the macromodel. Here, for the same DC voltage, responses with different amplitudes were obtained by applying the DC bias voltage in two steps. In the first step, a voltage V_{start} that is less than the desired DC bias, was applied and the simulation was done with damping until the beam reached the steady-state. In the second step, the damping was removed and an additional DC bias was applied to reach the desired DC voltage. The frequency of the signal resulting in the second step was measured. Different amplitudes were obtained by varying V_{start}. The variation of the frequency with the amplitude is shown in Figure 10. It can be seen here that the frequency decreases rapidly as the amplitude increases. This amplitude-softening at a given DC bias is also a consequence of the negative, nonlinear "electrostatic spring".

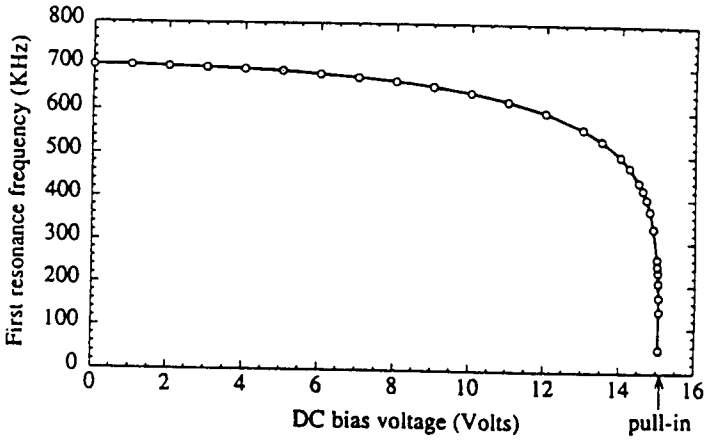

Figure 9 Frequency pull-in effect with DC bias

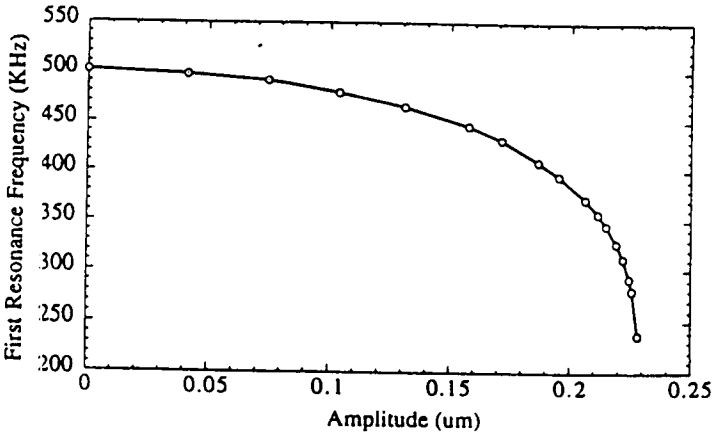

Figure 10 Amplitude dependence of the beam's resonance frequency at 14 V DC bias

Another consequence of the frequency-shift comes about when the driving frequency of the AC signal is varied. As opposed to the linear systems, here the amplitude does not go unbounded when the drive frequency is equal to the resonance frequency of the original state and there is no damping. Instead, we see beat phenomenon. These effects were all present in the simulation of the macromodels. Thus, there is no loss of detail due to the macromodeling procedure.

Simulation and measurement of time to pull in

Gupta et al. (1996a) reported the experimental data on the time required for the structure to contact the ground electrode when a voltage beyond the pull-in voltage is applied. This time is referred to as 'pull-in time', t_{pi}. The measurements were taken for the polysilicon beam whose physical and material property data is shown in Table 3. For different values of DC bias voltage applied as a step, t_{pi} was measured when the beam is set up in a vacuum of 6 μbar. The beam used in the experiment was fabricated using the MCNC's (1995) surface micromachining process (MUMPs), and has a compressive residual stress of 5MPa (Gupta et al., 1996a). The finite-element software ABAQUS was used to generate the mode shapes, the generalized mass matrix, and generalized stiffness matrix for the beam which included the effect of compressive residual stress. These were then used in the explicit dynamic simulation implemented in MATLAB.

The experimental and simulated data for t_{pi} at different non-dimensionalized voltages is shown in Figure 11. The voltage was non-dimensionalized by dividing the actual applied step voltage by the respective dynamic pull-in voltages. The non-dimensionalized voltage is used in this graph to emphasize the qualitative agreement between the experiment and the simulation. The dynamic pull-in voltages for the experiment and the simulation were 8.04V and 6.685V respectively. As explained earlier, the reasons for this discrepancy are thought to be the stress-stiffening effect and pre-buckled deformation of the beam under the effect of compressive residual stress. The conformal deposits used in the surface micromachining process give rise to 'compliant supports' (Gupta et al., 1996b) which cause the beam to bow up below the buckling stress. This change in geometry increases the gap between the structure and the ground electrode. The increase in the initial gap explains the higher pull-in voltages observed in the experiment. The stress-stiffening effect that was not included in the macro-model based simulation is another reason for larger values of pull-in voltages and t_{pi} in the experiment. The inclusion of these effects in the generation and simulation of the mode-based macromodel is in progress.

CONCLUSION

The linear normal mode summation method can be effectively used to generate macromodels to describe the electrostatic-elastomechanical dynamic behavior of the system. The added computational cost of transforming to the modal coordinates is small, but the computational advantage in simulation is enormous. The validity of the approach is illustrated with a simple example. The simulations are also shown to be in reasonable agreement with the experimentally measured values of pull-in voltages and the time for pull-in to occur. Based on these results, the normal mode based macromodels seem to provide an efficient method to simulate the nonlinear dynamics of Electrostatically actuated MEMS devices.

Length = 610 um
Width = w = 40 um
Thickness = t = 2.12 um
Initial gap = g_0 = 2.07 um
Young's modulus = E = 155 GPa
Poisson's ratio = 0.3
Mass density = ρ = 2300 Kg/m^3
Residual stress = -5.0 MPa (bi-axial)

Table 3 Physical and material properties of the MUMPs beam

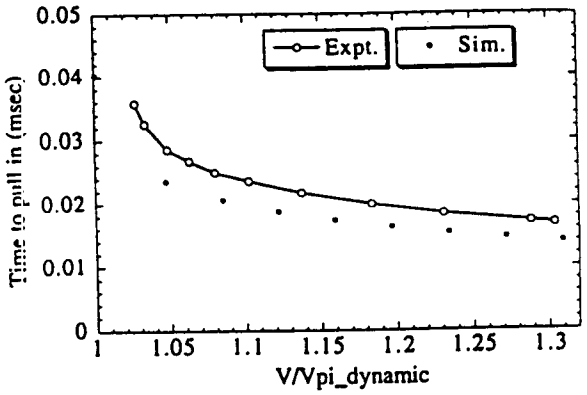

Figure 11 Comparison of experimental and simulated values of t_{pi} (time to pull in) at different voltages (the voltages shown in the graph are non-dimensionalized by dividing the actual applied step voltage by the respective dynamic pull-in voltage)

ACKNOWLEDGMENT

The authors thank Dr. John Gilbert, Microcosm Technologies Inc., Cambridge, MA, for many helpful discussions. This work was supported by ARPA under the contracts J-FBI-92-196 and J-FBI-95-215.

REFERENCES

ABAQUS, 1995, *ABAQUS User's Manual*, Version 5.5, HKS Inc., Pawtucket, RI.

Apte, R.B., Sandejas, F. S. A., Banyai, W. C., and Bloom D.M., 1994, "Deformable Grating Light Valves for High Resolution Displays," *Solid-State Sensor and Actuator Workshop*, Hilton Head, SC, 1994, pp. 1-6.

Gilbert, J.R., Ananthasuresh, G.K., and Senturia, S.D., 1996. "3D Modeling of Contact Problems and Hysteresis in Coupled

Electro-Mechanics," MEMS '96, *International Workshop on Micro Electro Mechanical Systems*, San Diego, CA, pp. 127-132.

Gupta, R. K., Hung, E., Yang, Y.-J., Ananthasuresh, G.K., and Senturia, S.D., 1996a, "Pull-in Dynamics of Electrostatically-Actuated Beams," Late News Poster Session Supplemental Digest at *Solid-State Sensor and Actuator Workshop*, Hilton Head, SC, 1996, pp. 1-2.

Gupta, R. K., Osterberg, P.M., and Senturia, S.D., 1996b, "Material Property Measurements of Micromechanical Polysilicon Beams," SPIE 1996 Conference (Invited Paper), Microlithography and metrology in Micromachining II, October 14-15, 1996.

MATLAB Reference Guide, The Math Works Inc., 1993

MCNC, 1995, MUMPs-5 (Multi-user MEMS Processes) service offered by Microelectronic Center of North Carolina, Research Triangle Park, NC.

Osterberg, P.M., Gupta, R.K., Gilbert, J.R., and Senturia, S.D., 1994, "Quantitative Models for the measurement of Residual Stress, Poisson's Ratio and Young's Modulus using Electrostatic Pull-in of Beams and Diaphragms," *Solid-State Sensor and Actuator Workshop*, Hilton Head, SC, 1994, pp. 184-188.

Przemienickie, J.S., 1968, "Theory of Matrix Structural Analysis," McGraw-Hill, New York, 1968, pp. 70-82.

Senturia, S.D., 1995, "CAD for Microelectromechanical Systems,", *Transducers '95*, Eurosensors IX, Stockholm, Sweden, 1995, Paper No. 232-A7, Vol. 2, pp. 5-8.

Shi, F., Ramesh, P., and Mukherjee, S., 1996, "Dynamic Analysis of Micro-Electro-Mechanical Systems (MEMS)," Preprint.

Spangler, L., and Kemp, C.J., 1995, "ISAAC (Integrated Silicon Automatic Accelerometer)," *Transducers '95*, Eurosensors IX, Stockholm, Sweden, 1995, Paper No. 147-C4, Vol. 1, pp. 585-588.

Thomson, W.T., 1988, "Theory of Vibrations with Applications," CBS Publishers, New Delhi, 1988, pp. 117-178.

Tilmans, A.C., 1993, "Micro-Mechanical Sensors Using Encapsulated Built-in Resonant Strain Gauges," *Ph.D. Dissertation*, The University of Twente, The Netherlands, 1993, pp. 152-154.

Ulrich, J., Füller, H., and Zengerle, R., 1995, "Static and Dynamic Flow Simulation of a KOH-Etched Microvalve," *Transducers '95*, Eurosensors IX, Stockholm, Sweden, 1995, Paper No. 235-A7, Vol. 2, pp. 17-20.